Interacting topological edge channels

Jonas Strunz,[1,2,*] Jonas Wiedenmann,[1,2,*] Christoph Fleckenstein,[3,*] Lukas Lunczer,[1,2] Wouter Beugeling,[1,2] Valentin L. Müller,[1,2] Pragya Shekhar,[1,2] Niccoló Traverso Ziani,[3,4] Saquib Shamim,[1,2] Johannes Kleinlein,[1,2] Hartmut Buhmann,[1,2] Björn Trauzettel,[3] and Laurens W. Molenkamp[1,2]

[1]*Experimentelle Physik III, Physikalisches Institut, Universität Würzburg, Am Hubland, D-97074 Würzburg, Germany*
[2]*Institute for Topological Insulators, Am Hubland, D-97074 Würzburg, Germany*
[3]*Institute of Theoretical Physics and Astrophysics, University of Würzburg, 97074 Würzburg, Germany*
[4]*Dipartimento di Fisica, Università di Genova, CNR-SPIN, Via Dodecaneso 33, 16146 Genova, Italy*

(Dated: June 24, 2019)

Electrical currents in a quantum spin Hall insulator are confined to the boundary of the system. The charge carriers can be described as massless relativistic particles, whose spin and momentum are coupled to each other. While the helical character of those states is by now well established experimentally, it is a fundamental open question how those edge states interact with each other when brought in spatial proximity. We employ a topological quantum point contact to guide edge channels from opposite sides into a quasi-one-dimensional constriction, based on inverted HgTe quantum wells. Apart from the expected quantization in integer steps of $2e^2/h$, we find a surprising additional plateau at e^2/h. We explain our observation by combining band structure calculations and repulsive electron-electron interaction effects captured within the Tomonaga-Luttinger liquid model. The present results may have direct implications for the study of one-dimensional helical electron quantum optics, Majorana- and potentially para-fermions.

The quantum spin Hall effect has been predicted in several systems [1–4] and was first realized in HgCdTe/HgTe quantum wells [5]. Later, this phase was observed in other material systems such as InAs/GaSb double quantum wells [6] and in monolayers of WTe_2 and bismuthene [7, 8]. The defining properties of this state, related to its helical nature, are well established by numerous experiments such as the observation of conductance quantization of two spin polarized edge channels $G_0 = 2e^2/h$ with e the electron charge and h the Planck's constant [5]. Additionally, non-local edge transport and spin-polarization of the edge channels were demonstrated by suitable transport experiments [9, 10]. In the present paper, we target a still open question, i.e. how helical edge states interact with each other.

A quantum point contact (QPC) can be used to guide edge channels from opposite boundaries of the sample into a constriction. Such a device allows for studies of charge and spin transfer mechanisms by, *e.g.*, adjusting the overlap of the edge states [11–21]. Besides the general interest in the study of transport processes in such a device, the appropriate model to describe the essential physics and to capture interaction effects of helical edge states is still unclear. The one-dimensionality of the helical edge modes suggests a description in terms of the Tomonaga-Luttinger liquid when electron-electron interactions are taken into account. In this respect, the QPC setup provides an illuminating platform as it may give rise to particular backscattering processes.

We present the realization of a QPC based on HgTe quantum wells as evidenced by the observation of the expected conductance steps in integer values of G_0. The newly developed lithographic process allows the fabrication of sophisticated nanostructures based on topological materials without lowering the material quality. It thus opens the path to conduct experiments of topological materials on mesoscopic scales important for the coherent control of helical edge channels and topological quantum computing. Depending on the QPC width W_{QPC} and quantum well thickness d_{QW}, we observe a fractional plateau at $0.5G_0$ in absence of an applied magnetic field. We label this phenomenon the *0.5 anomaly* in resemblance to the 0.7 anomaly frequently observed in point contacts fabricated in more conventional semiconductors [22]. Self-consistent $k \cdot p$ calculations allow us to identify the most plausible transport mechanism. Using the theory of helical Tomonaga-Luttinger liquids, we associate the experimental results with the presence of a spin-gap. Bias and temperature dependencies of the 0.5 anomaly are in agreement with such a gap. Furthermore, we identify an indicator of the conventional 0.7 anomaly in our devices when increasing the applied bias voltage. This observation is in qualitative agreement with the present theory and the explanation given for the 0.7 anomaly in Ref. [23].

*All three authors contributed equally to this work, email: Jonas.Strunz@physik.uni-wuerzburg.de

I. REALIZATION OF A QUANTUM SPIN HALL QUANTUM POINT CONTACT

Figure 1a shows a scanning electron micrograph picture of a HgTe QPC. A constriction is formed by wet chemical etching of the HgTe heterostructure [24] and a top gate electrode is used to tune the chemical potential [25]. The commonly employed approach of defining the QPC purely by electrostatic gating [26] is not suitable in our case due to the presence of gapless edge modes with linear dispersion (Klein tunnelling) [27].

Our devices are fabricated from HgTe quantum wells epitaxially grown on $Cd_{0.96}Zn_{0.04}Te$ substrates and sandwiched between $Hg_{0.3}Cd_{0.7}Te$ barriers (see inset Fig. 1b). The thickness of the HgTe layer, if not explicitly stated otherwise, is $d_{\mathrm{QW}} = 10.5\,\mathrm{nm}$. The width of the channel W_{QPC} ranges between 25 to 250 nm, while the length L_{QPC} is kept constant around 500 nm. The length of the gate electrode L_{Gate} is approximately 200-300 nm. As depicted in Fig. 1b, ohmic contacts are placed far away ($d_{\mathrm{ohmics}} \approx 80\,\mu\mathrm{m}$) from the constriction to allow full energy relaxation in the HgTe leads and to avoid geometrical resonances. Details about the fabrication process, material parameters and measurement setup are presented in the supplementary information, Sec. I.

The conductance G of a representative QPC as a function of applied gate voltage V_G is depicted in Fig. 1c. Three regimes can be identified. For gate voltages $V_G \geq -0.75\,\mathrm{V}$, we observe conventional QPC behaviour. Conductance plateaus at integer multiples of G_0 are developed and the quality of quantization can be improved by applying a small magnetic field (shown in red). For gate voltages between $-0.75\,\mathrm{V} > V_G > -1.2\,\mathrm{V}$ the point contact is in the quantum spin Hall regime. A long plateau around G_0 is assigned to two helical edge channels. For still more negative gate voltages $V_G \leq -1.2\,\mathrm{V}$, a step-like transition from G_0 to a long plateau at $0.5G_0$ is observed. The inset shows the remarkable precision of the quantization even at zero magnetic field. This observation constitutes the main finding of this work.

II. THE 0.5 ANOMALY

The 0.5 anomaly is a robust signature. It is stable over multiple thermal cycles and we have reproduced it in several devices. An overview of various devices is presented in Fig. 2. The 0.5 anomaly can be identified in devices number II to V, which have a constriction width of $W_{\mathrm{QPC}} = 100$-$200\,\mathrm{nm}$ (Fig. 2b-c). The conductance drops below G_0 but does not reach $0.5G_0$ for wider constrictions like in QPC-I, where $W_{\mathrm{QPC}} \approx 250\,\mathrm{nm}$ (Fig. 2a). This behaviour suggests that an interaction between the edge channels is crucial for the appearance of the 0.5 anomaly. The conductance of e^2/h implies the transmission of one channel while the other one is reflected. Preliminary data of the detection of this backscattered state is presented in the supplementary information, Fig. S3. In that experiment, adjacent voltage probes in a Hall geometry next to a QPC have been used to detect an emerging voltage drop with the QPC entering the 0.5 anomaly regime at $B = 0\,\mathrm{T}$. Our measurement of R_{xy} is consistent with predictions by Landauer-Büttiker theory for one reflected helical edge channel.

The conductance in the bulk band gap vanishes for very narrow QPCs as depicted in Fig. 2d ($W_{\mathrm{QPC}} \approx$ 25-50 nm). In this regime, the transport shows a Coulomb blockade behaviour typical for quantum dots (supplementary information, Fig. S2). We believe that inter-edge coupling and/or local disorder is responsible for the localization. The suppression of conductance for narrow QPCs sets an experimental upper limit for the wave function width of the edge states. Since we are still able to observe a G_0 plateau for $W_{\mathrm{QPC}} = 150\,\mathrm{nm}$ and no suppression of conductance inside the band gap for $W_{\mathrm{QPC}} = 100\,\mathrm{nm}$, we conclude that the localization of each edge channel has to be smaller than 50 nm, in agreement with theory [21]. In the QPCs with $W_{\mathrm{QPC}} = 100\,\mathrm{nm}$, shown in Fig. 2c, a plateau at G_0 is not visible anymore whereas the one at $0.5\,G_0$ can still be observed (to some extent). We attribute this behavior to stronger inter-edge interactions in narrower QPCs in our model described below in Sec. IV. The 0.5 anomaly is observed at large negative gate voltages over a wide voltage range. The gate efficiency in our devices is known from reference Hall bars to be $\Delta n_e/\Delta V \approx 8\text{-}10 \times 10^{11}\mathrm{cm}^{-2}/\mathrm{V}$. Therefore, we conclude that the bulk density in the regime of the 0.5 anomaly is strongly p-doped ($n_h > 1\times10^{12}\mathrm{cm}^{-2}$). Bulk transport through the point contact in this regime is suppressed, as will be further discussed below. As shown in Fig. 1c, a magnetic field $B \lessapprox 300\,\mathrm{mT}$ does not influence the 0.5 anomaly. The QPC conductance of a thinner, but still inverted HgTe quantum well ($d_{\mathrm{QW}} \approx 7.0\,\mathrm{nm} > d_c$) with $W_{\mathrm{QPC}} \approx 100\,\mathrm{nm}$ is shown in Fig. 2e. By lowering the gate voltage, first conventional conductance steps are observed. The lowest conductance in this device is around G_0 indicating the quantum spin Hall regime. We carefully checked that indeed no 0.5 anomaly is observed in thin quantum wells by studying several QPCs with varying W_{QPC}, measured in a large temperature (25 mK up to 10 K) and gate voltage range (see Fig. 2f). These findings guide us to the importance of the underlying band structure to identify the mechanism for the 0.5 anomaly.

III. BAND STRUCTURE CALCULATIONS

Using $k\cdot p$ theory based on the eight-band Kane model, we first calculate the bulk band structure of an infinitely wide slab of quantum well material (black curves in Fig. 3a-c) [28]. A more elaborated calculation using a finite width $W_{\mathrm{QPC}} = 150\,\mathrm{nm}$ of the system allows us to gain information about the situation inside the QPC constriction (coloured dots in the plots).

The band structure of a quantum well with $d_{\mathrm{QW}} =$

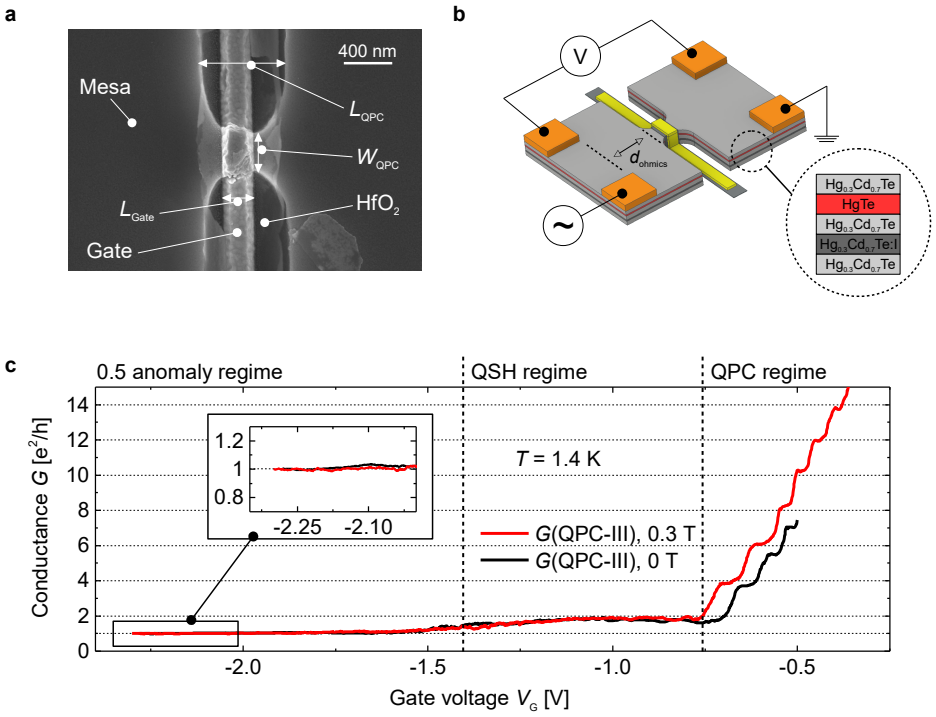

FIG. 1: **Realization of a topological quantum point contact: a**, Scanning electron micrograph of an exemplary device. A narrow channel is defined in the HgTe mesa with width W_{QPC} and length L_{QPC}. A metallic gate electrode is separated from the mesa by a HfO_2 dielectric. **b**, Schematic of the QPC design and measurement setup. The gate electrode is depicted in yellow and the ohmic contacts in orange. The inset shows the epitaxially grown layer stack on a commercially available $Cd_{0.96}Zn_{0.04}Te$ substrate. **c**, Gate voltage dependence of the conductance of QPC-III measured at 1.4 K. The conductance is divided into three regimes indicated by the vertical dashed lines. In the QPC regime, integer steps up to $14e^2/h$ are observed. The pure quantum spin Hall regime is defined by a conductance of $2e^2/h$ (abbreviated as QSH regime in **c**). In the 0.5 anomaly regime an interaction driven gap opens leading to a quantized conductance of e^2/h. The inset shows a zoom of the 0.5 anomaly regime.

7 nm (Fig. 3a) shows the inverted band gap between the $|H_1\pm\rangle$ and $|E_1\pm\rangle$ sub-bands as conduction and valence band, respectively. Importantly, the crossing point of the edge channels (Dirac point) lies in the bulk band gap. In contrast, the order of bands in the 10.5 nm wide quantum well is rather different (Fig. 3b). In this case, the band gap is between the first $|H_1\pm\rangle$ and second $|H_2\pm\rangle$ heavy hole sub-band. The $|E_1\pm\rangle$ sub-band – still responsible for the band inversion – lies energetically below the $|H_2\pm\rangle$ state. Then, the Dirac point is buried deeply in the valence band and the edge states hybridize with the bulk states if they spatially overlap [29]. However, at the indicated position of the chemical potential in Fig. 3c (by the dashed line), the edge states are well localized at the sample edge while the bulk density is already hole dominated. The corresponding edge wave function has a width of approximately 10 nm. This value is in qualitative agreement with our observation of unperturbed edge channel transport for QPC widths $W_{\mathrm{QPC}} \geq 100$ nm.

The position of the Dirac point in the valence band and the flat heavy hole bands have several implications for carrier transport. First, lowering the gate voltage in wider quantum wells pushes the chemical potential into the heavy hole $|H_2\pm\rangle$ bulk sub-bands, where the valence band structure exhibits a camel back-like shape. As a consequence, the Fermi level is pinned at the flat valence band edge. Second, the large Fermi momentum mismatch between valence and conduction band suppresses inter-band transitions and thus also suppresses bulk transport in the p-regime. In addition, the separation in momentum space between the edge and bulk states allows their coexistence without hybridization. These arguments explain the range in gate voltage of the quantum spin Hall plateau at G_0, which is longer than the 'conventional' steps, as well as the suppression of bulk conductance when entering the valence band. Furthermore, the application of a large negative gate voltage induces a strong Rashba effect. Self-consistent $k \cdot p$ calculations allow us to include the applied electric field and the resulting band structure is shown in Fig. 3c [28]. The dispersion of the bulk bands shows the typical Rashba splitting, while the dispersion of the edge states is not affected. The Rashba coupling does induce an energy dependence of the spin-momentum locking in the edge

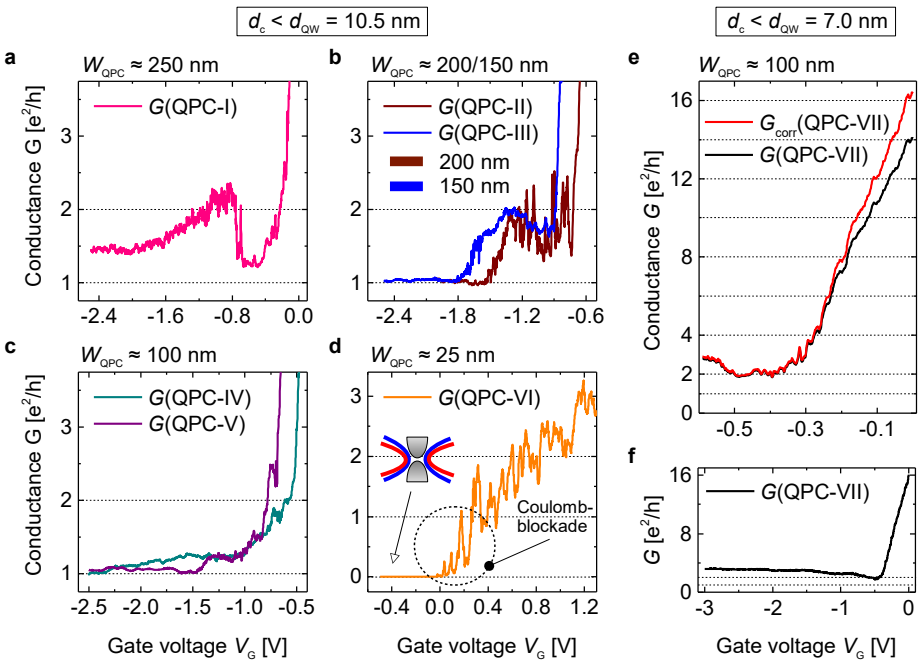

FIG. 2: **Width dependencies of the 0.5 anomaly: a-d**, Conductance as a function of gate voltage V_G measured at zero magnetic field and a temperature of $T \approx 1.4\,\mathrm{K}$ for QPCs with varying width W_{QPC} as indicated. The blue trace represents a second sweep of QPC-III. The shift in V_G compared to the data of Fig. 1c is due to hysteresis effects. **e-f**, Conductance of a QPC based on a quantum well width $d_{QW} = 7.0\,\mathrm{nm}$. The raw data is depicted in black, a serial resistance of $260\,\Omega$ was subtracted for the red graph. A wider gate voltage range is shown in the lower panel.

states as indicated by the tilted arrows [30, 31]. Obviously, a band splitting due to the Rashba coupling alone can not explain a 0.5 anomaly, since it does not break time reversal symmetry [32]. Hence, we have to take interactions into account.

IV. OPENING OF A SPIN GAP DUE TO COULOMB INTERACTIONS

In this section, we explain how the emergence of a spin gap generated by correlated two-particle scattering processes can explain the 0.5 anomaly. It is well known that the combination of Rashba spin-orbit coupling and electron-electron interactions at the helical edge can in principle give rise to backscattering (supplementary information, Sec. III) [33, 34]. When both edge channels interact with each other, a variety of two-particle scattering terms are allowed [13, 14, 19, 35]. In general, however, most of these terms are either not relevant in a renormalisation group sense, or do not apply to the constraints set by the band structure in our setup.

As indicated by the $k{\cdot}p$ calculations, the inverted quantum wells with $d = 10.5\,\mathrm{nm}$ have a Fermi wave vector of $k_F \sim 0.1\,\mathrm{nm}^{-1}$. Backscattering processes, which do not preserve the number of right- and left-moving edge channels, hence, oscillate as a function of space over a scale of k_F^{-1}. Since the length of the QPC is of the order of $L \sim 100\,\mathrm{nm}$, net effects of these terms should average out.

Following those arguments and assuming (weak) repulsive electron-electron interactions, we show in the supplementary information, Sec. III, that the most relevant two-particle scattering term can be written has

$$H_S = g_s \int_0^L dx[\hat{\chi}^\dagger_{R,+}(x)\hat{\chi}_{L,+}(x)\hat{\chi}^\dagger_{L,-}(x)\hat{\chi}_{R,-}(x) + \mathrm{h.c.}], \tag{1}$$

where $\hat{\chi}_{\nu,\pm}(x)$ with $\nu \in R, L$ are right- (R) and left-moving (L) Fermi field operators of upper ($+$) or lower edge ($-$), respectively. Since the spin degree of freedom and the direction of motion are pinned in each helical liquid, we only indicate the direction of motion in Eq. (1) and drop the spin degree of freedom for ease of notation. Evidently, H_S describes a backscattering process between the ($+$) and ($-$) edges preserving the number of right- and left movers (see Fig. 3d for a schematic).

In our minimal model, introduced in the supplementary information, Sec. III, Eq. (1) appears due to the combination of Rashba spin-orbit coupling and electron-electron interactions with broken SU(2) symmetry of the spin degree of freedom. The coupling constant g_s

$$g_s = \sin^2(\gamma)\frac{g_{2\perp} - g_{4\perp}}{2} \tag{2}$$

is found to be directly related to the magnitude of the Rashba coupling strength α via $\gamma = \arctan[\alpha/(\hbar v_F)]$,

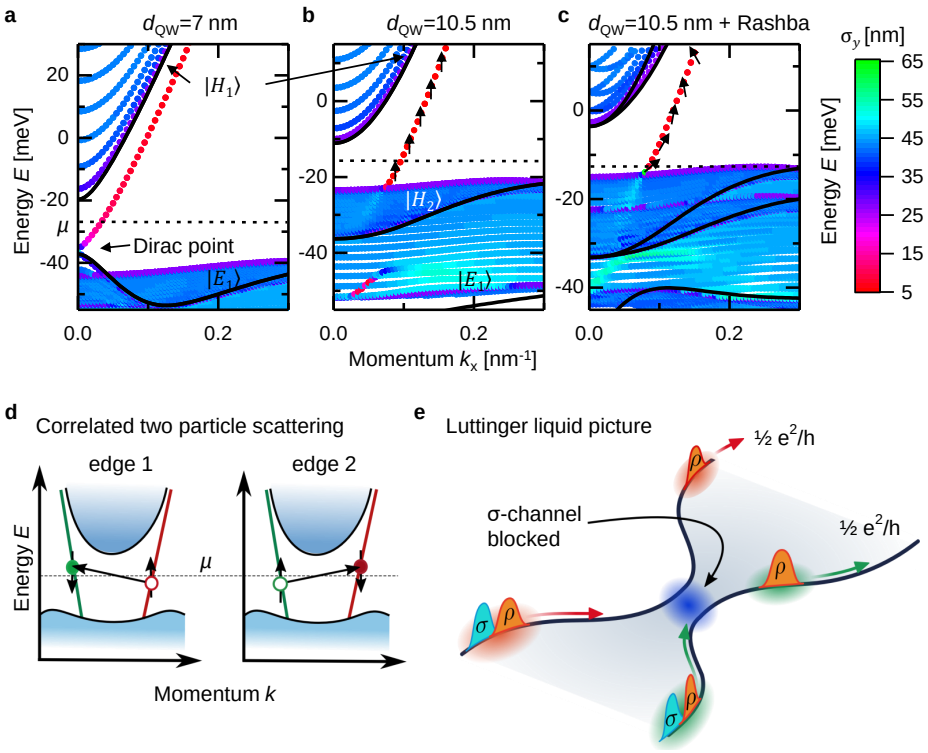

FIG. 3: $k \cdot p$ **band structure calculations and illustrations of the scattering process: a-c**, Black lines indicate the bulk band structure. The coloured dots present calculations performed on a finite ribbon with a width of 150 nm in the y direction. The colour code shows the wave function standard deviation σ_y in the y direction. Small values (red) indicate strongly localized states, large values (blue) bulk like states. Panel **a** shows the calculated band structure of a 7.0 nm quantum well. The Dirac point lies in the bulk band gap. Panel **b** and **c** show the band structure for a 10.5 nm thick quantum well. Realistic finite electric fields have been applied to the quantum well on the bottom (to simulate iodine doping) and on the top (gate electrode) in panel **c**, which introduces a Rashba effect as well as a tilting of the spin polarization of the helical edge states away from the normal, as sketched by the arrows. **d**, Schematic of the correlated scattering process, responsible for the spin gap. **e**, Illustration of the reduction of conductance in the Tomonaga-Luttinger liquid picture, where σ and ρ indicate the bosonic charge and spin fields.

as well as to the electron-electron interaction processes across the edges parametrized by $g_{2\perp}$ and $g_{4\perp}$. In the presence of strong spin-orbit coupling, SU(2) invariance is broken at the single-particle level. Hence, it makes sense that it remains to be broken in the presence of interactions which implies that $g_{2\perp} \neq g_{4\perp}$.

The Fermi level pinning in the samples with quantum well thickness of 10.5 nm, thus, allows the coupling constant g_s to grow, as the electric field and likewise the Rashba coupling is increased. This indicates the importance of the camel back in the bandstructure shown in Fig. 3 **c** for the development of a sufficiently large g_s.

Using bosonization techniques, we can demonstrate that Eq. (1) acts as a gap to the spin sector[36]. The effective Hamiltonian reads

$$H_{\text{eff}} = \frac{1}{2\pi}\int_0^L \mathrm{d}x \sum_{\nu=\sigma,\rho}\left[\frac{u_\nu}{K_\nu}\left(\partial_x\phi_\nu\right)^2 + u_\nu K_\nu \left(\partial_x\theta_\nu\right)^2\right] + \tilde{g}_s\cos(2\sqrt{2}\theta_\sigma), \quad (3)$$

where $\phi_\nu(x)$, $\theta_\nu(x)$ $(\nu \in \rho,\sigma)$ describe bosonic fields acting on spin (σ) and charge sector (ρ), $\tilde{g}_s$ is a rescaled version of g_s, u_ν represent the normalised velocities and K_ν are the Tomonaga-Luttinger interaction parameters ranging between $0 \leq K_\rho \leq 1$ and $1 \leq K_\sigma \leq 1/K_\rho$ for a repulsively interacting system. We have dropped the explicit spatial dependence of the bosonic fields for ease of notation. The last term in Eq. (3) – proportional to $\tilde{g}_s$ – corresponds to a gap in the spin sector. In the supplementary information, Sec. III, we explain that (in a mean-field sense) the emergence of the spin gap can be understood as spontaneous time-reversal symmetry breaking.

V. EXPERIMENTAL CONSEQUENCES OF A SPIN GAP

Usually, spin gaps are not detectable in charge transport experiments of purely one-dimensional systems. However, the strong localization of the single-particle wave functions at the edges of the QPC implies that in the present case the system is by no means a single one-dimensional system, but has to be treated as two spatially

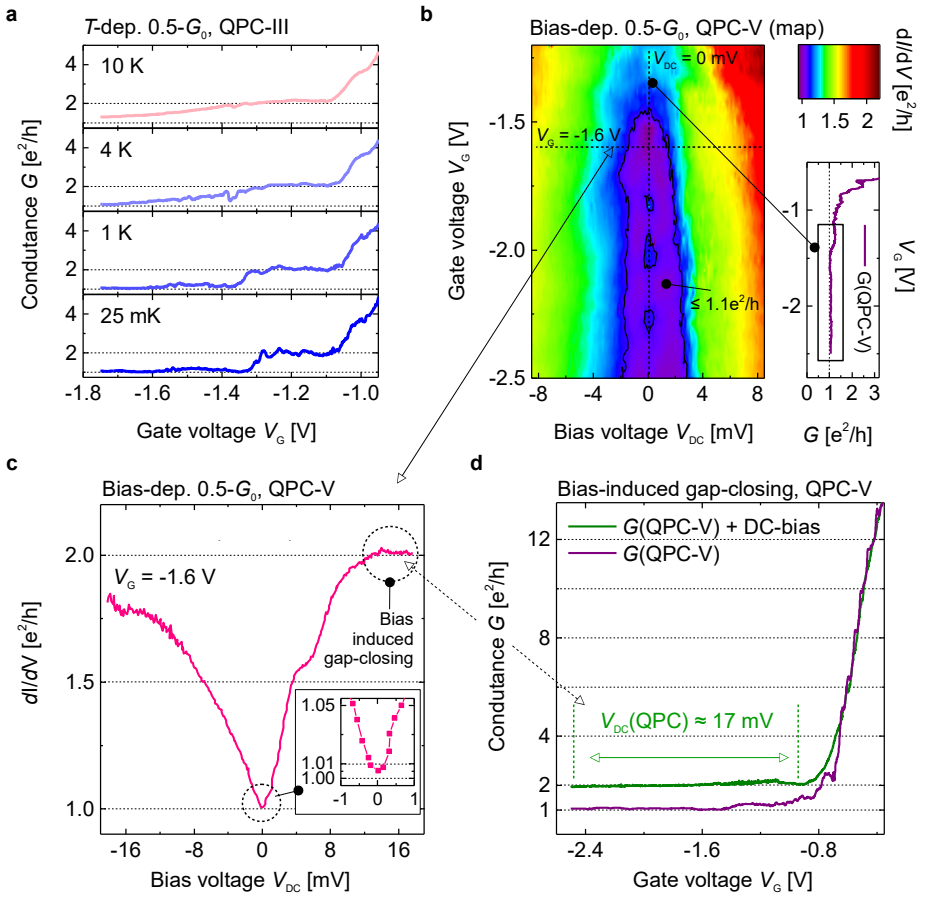

FIG. 4: **Temperature and dc bias dependence of the 0.5 anomaly: a**, Temperature dependence of the $2e^2/h$ to e^2/h transition of QPC-III. **b**, Differential conductance map of QPC-V as a function of bias and gate voltage. The violet area indicates the regime of the 0.5 anomaly. **c**, Line cut of the bias dependence at $V_G = -1.6\,\mathrm{V}$. We attribute the asymmetry of the bias dependence to self-gating effects. **d**, Conductance as a function of gate voltage of QPC-V for zero applied DC bias (violet) and large (green) applied DC bias of 17 mV.

separated one-dimensional systems, coupled by Coulomb interactions.

Thus, the current operators $j_\pm(x) = 1/(2\pi)\partial_t(\phi_\rho(x) \mp \theta_\sigma(x))$, where the index $\pm$ also relates to different y-coordinates, are distinct at the two edges. An electric bias couples to each helical edge state separately. This assumption leads to a reduced conductance of $G = 0.5G_0$ in the presence of a spin gap (see also Fig. 3e). In the absence of the spin gap, we instead find $G = G_0$ (supplementary information, Sec. III).

As observable in Fig. 2, the fluctuations on top of the 0.5 anomaly plateau are considerably smaller than in the quantum spin Hall regime, where both helical channels are transmitted. In the presence of Eq. (1), our renormalisation group analysis (supplementary information, Sec. III) indeed predicts a reduced sensitivity to impurity backscattering consistent with this observation. Moreover, we note that the proposed mechanism is not affected by magnetic fields, also consistent with the experiment.

The absence of the 0.5 anomaly in thinner quantum wells can be understood through the lack of Fermi level pinning. In thicker quantum wells (10.5 nm), the application of a strong electric field allows us to generate a sufficiently large Rashba field without substantially affecting the electron density of the edge states. The reason is that the camel back of the valence band has a large density of states at the Fermi energy which gives rise to Fermi level pinning, see the horizontal dashed line in Fig. 3c. In contrast, in thinner quantum wells (7 nm), the camel back is far away (in energy) from the Fermi level, see the horizontal dashed line in Fig. 3a. Hence, in that case, we are not able to apply strong electric fields without substantially affecting the electron density of the edge states. We argue that the resulting Rashba field, acting on the edge states in the transport regime with conductance $2e^2/h$, is too small to observe the 0.5 anomaly.

The bias and temperature dependence of the conductance, depicted in Fig. 4, helps us to quantify the observed energy scales. As shown in Fig. 4a, the 0.5 anomaly is observable up to temperatures of 1.4 K. For

higher temperatures ($T \geq 4\,\mathrm{K}$) the quantization is lost and the conductance increases with increasing temperatures. The range 1-2 K as the upper limit to which the quantized plateau is observed sets an energy scale of the spin gap $\Delta E \approx$ 150-300 µeV. This energy scale is in good agreement with the bias dependence shown in Fig. 4b. There, the low ac bias has been superimposed by a dc bias voltage V_{DC}. The gate voltage regime in which the 0.5 anomaly can be observed opens around $V_G = -1.6\,\mathrm{V}$. We are able to observe the 0.5 anomaly up to $V_{\mathrm{DC}} \approx$ 200-400 µeV (Fig. 4c) depending on the gate voltage. A similar estimate can be made for the energy scale set by the length of the QPC $\hbar v_F / L_{\mathrm{Gate}} \approx$ 200-300 µeV. The agreement of the magnitudes of all energy and temperature scales is remarkable. We conjecture that they set the typical energy scale required for the development of the 0.5 anomaly. For larger energies, the renormalisation group flow of g_s is stopped too early such that the spin gap can not develop.

Increasing the applied bias voltage further, the conductance increases beyond the 0.5 anomaly and a second step like plateau is visible around $\approx 0.8G_0$ (Fig. 4c). We conjecture that this feature is related to the 0.7 anomaly commonly observed in conventional QPCs. The emergence of this conventional 0.7-like signature is in qualitative agreement with the explanation given in Refs. [23, 37, 38] for GaAs based structures. In these articles, electron-electron interactions at the bottom of the last sub-band suppress the conductance below G_0. In our case, the 0.7 feature occurs where the applied bias becomes large enough to touch the bottom of the interaction induced gap. Depending on the device, we are also sometimes able to identify a 0.7 feature as a function of gate voltage (see Fig. 2b). Increasing the bias even further closes the interaction induced gap and the conduction saturates at G_0, *i.e.* two unperturbed edge channels are now perfectly transmitted through the QPC over a large range of gate voltage (see Fig. 4c-d).

Several other mechanisms might explain the 0.5 anomaly in QPCs or nanowires. These mechanisms include helical edge reconstruction [39], the formation of a Wigner crystal [40], or hyperfine interactions [41]. However, given the importance of the camel back in the valence band for our observation of the 0.5 anomaly, we believe that the mechanism presented here is the most plausible one. At the same time, we note (and discuss this more extensively in the supplementary information) that one can imagine another relevant mechanism, in particular, the helical edge reconstruction proposed in Ref. [39], that shares many common ingredients to our mechanism – like strong spin-orbit coupling, electron-electron interactions, and confinement. Hence, it is likely that the two mechanisms are related to each other (from a more fundamental point of view). Importantly, the explanation of the 0.5 anomaly relies in any case on the spontaneous breaking of time-reversal symmetry by interactions.

VI. SUMMARY & OUTLOOK

To conclude, we have presented the realization and operation of a QPC in a two-dimensional topological insulator. The conductance as a function of applied gate voltage saturates on a robust and reproducible $0.5G_0$ plateau. Investigations of this 0.5 anomaly for various QPC channel widths, combined with the fact that the 0.5 feature is linked to a certain quantum well thickness, gives a hint to the importance of the underlying band structure. Especially, the difference between a Dirac point in the band gap and one buried in the valence band guides us to a scattering term, which implies the opening of a spin gap. The 0.5 anomaly yields an effectively spin-polarized current, which may find applications in spintronics. Furthermore, the results could be important for the detection of Majorana bound states since the identified mechanism might be related to the observation of the 4π-periodic Josephson current in our HgTe Josephson junctions in the absence of an explicit time reversal symmetry breaking mechanism [42]. Combining a topological QPC with superconductors is envisaged to enable the creation and manipulation of Majorana bound states and parafermions [43, 44].

[1] F. D. M. Haldane, Phys. Rev. Lett. **61**, 2015 (1988).
[2] C. L. Kane and E. J. Mele, Phys. Rev. Lett. **95**, 226801 (2005).
[3] C. L. Kane and E. J. Mele, Phys. Rev. Lett. **95**, 146802 (2005).
[4] B. A. Bernevig, T. L. Hughes, and S.-C. Zhang, Science **314**, 1757 (2006).
[5] M. König, S. Wiedmann, C. Brüne, A. Roth, H. Buhmann, L. W. Molenkamp, X. L. Qi, and S.-C. Zhang, Science **318**, 766 (2007).
[6] I. Knez, R.-R. Du, and G. Sullivan, Phys. Rev. Lett. **107**, 136603 (2011).
[7] S. Wu, V. Fatemi, Q. D. Gibson, K. Watanabe, T. Taniguchi, R. J. Cava, and P. Jarillo-Herrero, Science **359**, 76 (2018).
[8] F. Reis, G. Li, L. Dudy, M. Bauernfeind, S. Glass, W. Hanke, R. Thomale, J. Schäfer, and R. Claessen, Science **357**, 287 (2017).
[9] A. Roth, C. Brüne, H. Buhmann, L. W. Molenkamp, J. Maciejko, X. L. Qi, and S.-C. Zhang, Science **325**, 294 (2009).
[10] C. Brüne, A. Roth, H. Buhmann, E. M. Hankiewicz, L. W. Molenkamp, J. Maciejko, X. L. Qi, and S.-C. Zhang, Nat. Phys. **8**, 486 (2012).
[11] C.-Y. Hou, E.-A. Kim, and C. Chamon, Phys. Rev. Lett. **102**, 076602 (2009).
[12] A. Ström and H. Johannesson, Phys. Rev. Lett. **102**, 096806 (2009).
[13] J. C. Y. Teo and C. L. Kane, Phys. Rev. B **79**, 235321 (2009).

[14] Y. Tanaka and N. Nagaosa, Phys. Rev. Lett. **103**, 166403 (2009).
[15] F. Dolcini, Phys. Rev. B **83**, 165304 (2011).
[16] V. Krueckl and K. Richter, Phys. Rev. Lett. **107**, 086803 (2011).
[17] L. B. Zhang, F. Cheng, F. Zhai, and K. Chang, Phys. Rev. B **83**, 081402 (2011).
[18] C. P. Orth, G. Strübi, and T. L. Schmidt, Phys. Rev. B **88**, 165315 (2013).
[19] P. Sternativo and F. Dolcini, Phys. Rev. B **89**, 035415 (2014).
[20] F. Dolcini, Phys. Rev. B **92**, 155421 (2015).
[21] M. Papaj, L. Cywiński, J. Wróbel, and T. Dietl, Phys. Rev. B **93**, 195305 (2016).
[22] A. P. Micolich, J. Phys.: Condens. Matter **23**, 443201 (2011).
[23] F. Bauer, J. Heyder, E. Schubert, D. Borowsky, D. Taubert, B. Bruognolo, D. Schuh, W. Wegscheider, J. V. Delft, and S. Ludwig, Nature **501**, 73 (2013).
[24] K. Bendias, S. Shamim, O. Herrmann, A. Budewitz, P. Shekhar, P. Leubner, J. Kleinlein, E. Bocquillon, H. Buhmann, and L. W. Molenkamp, Nano Lett. **18**, 4831 (2018).
[25] A. Kristensen, J. B. Jensen, M. Zaffalon, C. B. Sorensen, S. M. Reimann, P. E. Lindelof, M. Michel, and A. Forchel, J. Appl. Phys. **83**, 607 (1998).
[26] B. J. van Wees, H. van Houten, C. W. J. Beenakker, J. G. Williamson, L. P. Kouwenhoven, D. van der Marel, and C. T. Foxon, Phys. Rev. Lett. **60**, 848 (1988).
[27] M. I. Katsnelson, K. S. Novoselov, and A. K. Geim, Nat. Phys. **2**, 620 (2006).
[28] E. G. Novik, A. Pfeuffer-Jeschke, T. Jungwirth, V. Latussek, C. R. Becker, G. Landwehr, H. Buhmann, and L. W. Molenkamp, Phys. Rev. B **72**, 035321 (2005).
[29] R. Skolasinski, D. I. Pikulin, J. Alicea, and M. Wimmer, Phys. Rev. B **98**, 201404 (2018).
[30] T. L. Schmidt, S. Rachel, F. von Oppen, and L. I. Glazman, Phys. Rev. Lett. **108**, 156402 (2012).
[31] L. Ortiz, R. A. Molina, G. Platero, and A. M. Lunde, Phys. Rev. B **93**, 205431 (2016).
[32] L. W. Molenkamp, G. Schmidt, and G. E. W. Bauer, Phys. Rev. B **64**, 121202 (2001).
[33] H.-Y. Xie, H. Li, Y.-Z. Chou, and M. S. Foster, Phys. Rev. Lett. **116**, 086603 (2016).
[34] M. Kharitonov, F. Geissler, and B. Trauzettel, Phys. Rev. B **96**, 155134 (2017).
[35] C.-X. Liu, J. C. Budich, P. Recher, and B. Trauzettel, Phys. Rev. B **83**, 035407 (2011).
[36] T. Giamarchi, *Quantum Physics in One Dimension*, International Series of Monographs on Physics (Oxford University Press, Oxford, 2003).
[37] A. M. Lunde, A. De Martino, A. Schulz, R. Egger, and K. Flensberg, New J. Phys. **11**, 023031 (2009).
[38] C. Sloggett, A. Milstein, and O. Sushkov, Eur. Phys. J. **61**, 427 (2008).
[39] J. Wang, Y. Meir, and Y. Gefen, Phys. Rev. Lett. **118**, 046801 (2017).
[40] K. A. Matveev, Phys. Rev. Lett. **92**, 106801 (2004).
[41] C.-H. Hsu, P. Stano, J. Klinovaja, and D. Loss, Phys. Rev. B **97**, 125432 (2018).
[42] E. Bocquillon, R. S. Deacon, J. Wiedenmann, P. Leubner, T. M. Klapwijk, C. Brüne, K. Ishibashi, H. Buhmann, and L. W. Molenkamp, Nat. Nanotechnol. **12**, 137 (2016).
[43] J. Li, W. Pan, B. A. Bernevig, and R. M. Lutchyn, Phys. Rev. Lett. **117**, 046804 (2016).
[44] C. Fleckenstein, N. T. Ziani, and B. Trauzettel, Phys. Rev. Lett. **122**, 066801 (2019).

Acknowledgements

We like to thank E. Bocquillon, T. Borzenko, Y. Gefen, C. Gould, A. Currie, V. Hock, P. Leubner, and Y. Meir for fruitful discussions. We acknowledge financial support by the DFG (SPP1666 and SFB1170 "ToCoTronics"), the ENB Graduate school on "Topological Insulators", the EU ERC-AG Program (project 4-TOPS), and the Würzburg-Dresden Cluster of Excellence on Complexity and Topology in Quantum Matter (EXC 2147, project-id 39085490). C.F. acknowledges support from the Studienstiftung des Deutschen Volkes.

Author Contributions

J.S. prepared the samples and performed the experiments. V.M. and P.S. contributed to implement the fabrication process, S.S. and J.W. helped to do the measurements. J.K. supervised the sample fabrication. J.W. guided the experiments. L.L. grew the material. W.B. provided the code for the band structure calculations. C.F., N.T.Z. and B.T. developed the theoretic model. H.B. and L.W.M. planned the project and design of the experiment. All authors participated in the analysis of the data, led by J.S. and J.W. All authors jointly wrote the manuscript, led by J.W.

Competing interests

The authors declare that they have no competing financial interests.

Data availability

The data that support the plots within this paper and other findings of this study are available from the corresponding author upon reasonable request.